Vibrational Spectra and Density Functional Calculations of Bridged [14]Annulenes with an Anthracene Perimeter

Laura Moroni, Cristina Gellini, and Pier Remigio Salvi*

Dipartimento di Chimica, Universitá di Firenze, via della Lastruccia 3, 50019 Sesto Fiorentino, Firenze, Italy

Chung-Jing Liu and Emanuel Vogel

Institut für Organische Chemie, Universität zu Köln, Greinstrasse 4, 50939 Köln, Germany

Received: January 23, 2002; In Final Form: May 6, 2002

Vibrational spectra of two representative bridged [14]annulenes with an anthracene perimeter, 1,6:8,13-ethane-1,3-diylidene[14]annulene and 1,6:8,13-propane-1,3-diylidene[14]annulene (**4** and **5** in Figure 1, respectively), are presented and discussed on the basis of density functional calculations with the B3LYP functional and 6-31G** and cc-pVDZ basis sets. Infrared and Raman spectra of polycrystalline samples have been measured at room temperature. The Raman spectra have been obtained exciting at 647.1 and 1064 nm, that is, in pre- and off-resonance excitation conditions, respectively. Calculated structures of **4** and **5** are aromatic according to geometric criteria of aromaticity. Observed vibrational frequencies and infrared and Raman intensities of **4** and **5** are well reproduced by the present calculation using scaling factors of linearly condensed aromatic hydrocarbons taken from the literature. A correlation between vibrational modes of anthracene and ring modes of **4** and **5** is attempted in agreement with the aromatic nature of the [14]annulene ring. The effect of reduced symmetry and bridge structure on infrared and Raman intensities is discussed.

I. Introduction

The Hückel molecular orbital theory of benzene, according to which aromatic character is general for cyclically conjugated ring systems containing $(4n + 2)$ π electrons and being planar, provided the impetus for the development of annulenes and their chemistry.[1,2] It was Sondheimer who pioneered the synthesis of an almost complete series of annulenes ranging from [12]- to [30]annulene.[3] The properties of these and other annulenes, especially those of the rigid bridged-type,[4−6] vindicated theory most impressively.

Because [10]annulene represents the next higher, potentially aromatic homologue of benzene, it was a prime synthetic goal. Among the various stereoisomers of [10]annulene conceivable, the all-cis and the mono-trans isomers could be made but turned out to be reactive polyolefins.[7] Evidently, because of steric constraints, these molecules pronouncedly deviate from planarity. In striking contrast to the parent [10]annulene, 1,6-methano-[10]annulene (**1** in Figure 1), as well as its 1,6-epoxy and 1,6-imino analogues, in which the bridge compels the 10-membered ring to adopt a near planar conformation, qualify as aromatic molecules.[8]

It is a special feature of the "Hückel-aromatic" **1** that it bears a formal relationship to the classical aromatic hydrocarbon naphthalene. This relationship invited the synthesis of *syn*-1,6:8,13-bismethano[14]annulene (**2**) and its anti isomer (**3**) possessing anthracene perimeters.[9,10] As anticipated, it is the conformation of the perimeters of these molecules that determines their π-electron structure: the syn isomer, though slightly bent because of the steric interference of the inner bridge hydrogen atoms, is aromatic, whereas the anti isomer, existing as a fluxional molecule, suffers loss of aromaticity because of severe distortion of the C_{14} perimeter.

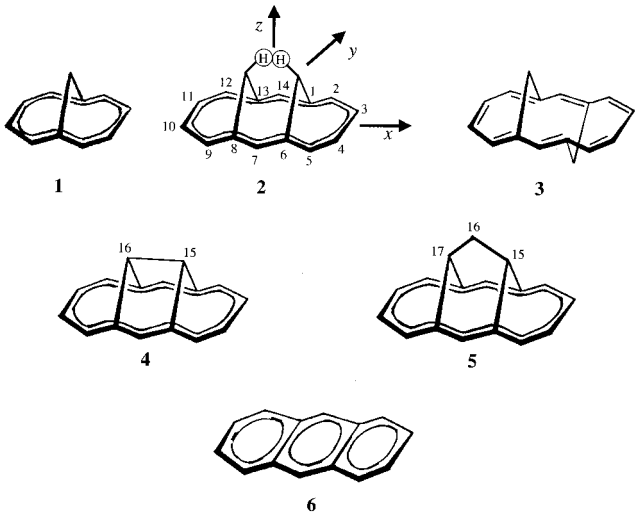

Figure 1. Molecular structures of 1,6-methano[10]annulene (**1**), *syn*-1,6:8,13-bismethano[14]annulene (**2**), *anti*-1,6:8,13-bismethano[14]-annulene (**3**), 1,6:8,13-ethane-1,3-diylidene[14]annulene (**4**), 1,6:8,13-propane-1,3-diylidene[14]annulene (**5**) and anthracene (**6**). The atomic numbering of the ring C atoms and the molecular reference system are common to the six molecules and shown for convenience only for **2**. Additional C atoms of **4** and **5** forming the bridge are explicitly numbered.

Two other bridged [14]annulenes, being very rigid and thus particularly relevant to the present work, derive from **2** by proper manipulation of the CH_2-bridges. Removal of the inner bridge hydrogen atoms with formation of a carbon−carbon bond leads to 1,6:8,13-ethane-1,3-diylidene[14]annulene (**4**), which exhibits a C_{14} perimeter flattened out almost completely.[11] Thus, **4** suggests a comparison with planar anthracene (**6**). If, on the other hand, the inner hydrogen atoms of **2** are replaced by a

* To whom correspondence should be addressed.

10.1021/jp020221m CCC: $22.00
Published on Web 06/21/2002

CH_2 group one arrives at 1,6:8,13-propane-1,3-diylidene[14]-annulene (**5**), matching **2** in that it possesses a slightly bent C_{14} perimeter.[12] Both **4** and **5** are perfectly stable aromatic molecules. Thus, it appears that the deviation of the C_{14} perimeters in **5** and **2** from planarity does not impair the π-electron delocalization profoundly.

Physical investigations on the "more-or-less planar" bridged [10]- and [14]annulenes discussed above have focused on X-ray structure determinations[13−16] and evaluation of the electronic spectra.[17−21] It occurred to our group that a study of the vibrational dynamics of these molecules through analysis of the infrared and Raman spectra will essentially contribute to their characterization. In fact, recently, we have reported on ground-state structural and vibrational properties of 1,6-methano- and 1,6-epoxy[10]annulene.[22] In particular, both frequency and intensity calculations based on the density functional (DF) approach were considered for the vibrational assignment. The importance of the DF method for vibrational assignment has been already emphasized in several papers.[23−25] In addition, in our study Raman intensities, which have not been usually considered so far in DF vibrational calculations, were in excellent agreement with experimental data. Following this procedure, the correlation between ring modes of bridged [10]annulenes and naphthalene modes was proposed.

Encouraged by these results, we have extended the vibrational analysis to two representative molecules of the bridged[14]-annulene series, 1,6:8,13-ethane-1,3-diylidene[14]annulene and 1,6:8,13-propane-1,3-diylidene[14]annulene (**4** and **5** of Figure 1, respectively). Experimentally, the infrared and Raman spectra of **4** and **5** have been measured on solid samples. Because of the visible absorption of both molecules,[19,20] Raman spectra have been observed in off- and preresonance conditions, at 1.06 μm and 647.1 nm, respectively. From the computational point of view, DF calculations have been performed using the 6-31G** and the correlation-consistent Dunning cc-pVDZ basis sets, as recently recommended for vibrational calculations.[23]

II. Experimental Section

The [14]annulenes **4** and **5** have been prepared following the reported synthetic routes.[11,12] Compound **4** was purified by chromatography on a basic alumina column using dichloromethane as the eluent and then recrystallized from benzene−hexane (1:2) to give a red crystalline solid with melting point 118−119 °C. On recrystallizing of **5** from dichloromethane−ethanol (1:2), a stable yellow crystalline solid is obtained with melting point 180−181 °C. The ^{1}H NMR spectra of **4** and **5**, consisting of the anticipated absorption pattern for the annulene and bridge protons, respectively, were in agreement with previous reports.[11,12] Both samples were stored at −10 °C in the dark until use.

Thin polycrystalline films of **4** and **5** were prepared for infrared measurements by melting the material between two CsI windows. The sample thickness was only approximately constant from one experiment to the other because of the window surfaces, not optically flat, and of the slightly varying melt compression. The IR spectra were measured at room temperature between 200 and 3500 cm^{-1} on a FTIR interferometer (Bruker, model IFS 120 HR) under medium resolution conditions, $\Delta\nu \approx 1$ cm^{-1}. The spectral region 200−3500 cm^{-1} was scanned using two different beam splitters (mylar and KBr, below and above 500 cm^{-1}, respectively). A few more spectra of **4** in KBr pellets were taken in the range 500−3500 cm^{-1}, similar to those of **4** as a film, though of lower spectral quality.

Because both solids absorb in the visible,[19,20] it was necessary to run the Raman spectra with excitation wavelength in the red or in the near-infrared. With excitation at 647.1 nm with the red line of a Kr^+ laser, the Raman spectra of **4** and **5** were taken between 20 and 1800 cm^{-1} with standard collection instrumentation (double monochromator, $\Delta\nu \approx 3$ cm^{-1}, red-extended cooled photomultiplier, photon-counting detection system). The sample was placed as a polycrystalline powder on the hollow tip of a metallic holder and irradiated with the mildly focused laser beam. With a laser power of ∼30 mW, no damage was visually detected on the sample surface, nor did the Raman signal change with time. The Raman spectrum of anthracene, which was also taken, was run under the same experimental conditions and found essentially coincident with most recent results.[26] The second Raman spectrum of **4** and **5** was measured by shifting the excitation wavelength to 1.06 μm, far from the lowest electronic absorption of both systems, with the FT/Raman option of the Bruker interferometer. In this case, the laser power was 150 mW and the resolution $\Delta\nu \approx 2$ cm^{-1}.

III. Results

A. Density Functional Calculations. The molecular structures of **4** and **5** were optimized by means of ab initio DF calculations as implemented in the Gaussian program[27] using the B3LYP exchange−correlation functional[28,29] with the 6-31G** and the cc-pVDZ basis sets. For both systems, a C_{2v} geometry is predicted, whichever the basis set, as expected from simple considerations about the aromatic nature of the two molecules and in agreement with X-ray diffraction data on **5**[16] and on the 15,16-dimethyl derivative of **4**.[30] In the latter case, it is assumed that the ring conformations of **4** and of its derivative are nearly identical, as suggested from their UV/vis spectra, which are virtually superimposable.[31] The ring bond lengths of **2**, **4**, **5**, and **6** (see Figure 1) are collected in Table 1. In the case of **2** and **6**, our values agree well with reported calculations.[23,32] The comparison with available experimental data[15,16,30,33] is shown in the same Table. Two geometric criteria of aromaticity have been generally proposed in the past years.[32,34,35] The first of these is based on the Julg parameter, $A = 1 - (225/n)\sum_i[1 - (r_i/r)]^2$, a measure of bond length alternation, where n is the number of C−C bonds involved in the conjugation (14 in our case), r_i is the length of the ith C−C bond, and r is the mean value.[35] A is unity for the fully delocalized benzene structure ($r_i = r$). To have $A = 0$ for the hypothetical localized form with full bond alternation between 1.33 and 1.52 Å, the multiplying factor (225/n) should be set in front of the sum in the definition of A. The second important parameter is Δr_m, the maximum deviation in absolute value of the C−C bond lengths from the mean. Aromatics have $\Delta r_m \leq 0.05$.[32] The two parameters, calculated from the optimized geometries of the four molecules and reported in Table 1, predict a reduced bond length alternation of **4** and **5** with respect to **6**. Also, there is a good consistency between experimental and calculated A and Δr_m values of **2**, **4**, **5**, and **6**.

To go now to discuss the vibrational dynamics of the two bridged [14]annulenes, the 78 vibrational modes of **4** are classified under C_{2v} symmetry as $22A_1 + 18A_2 + 19B_1 + 19B_2$, while those of **2**, 87 modes, are classified as $25A_1 + 19A_2 + 21B_1 + 22B_2$. If the interaction between ring and bridge internal coordinates is sufficiently small, the 12 bridge modes of **4**, that is, $4A_1 + 2A_2 + 4B_1 + 2B_2$, may be described in simple terms. If we denote as C_b the two C atoms of the bridge (C_{15} and C_{16}), the bridge modes are two C_bH stretchings (sym + asym; $A_1 + B_1$), one C_bC_b stretching (A_1), two C_bC_bH bendings (sym + asym; $A_1 + B_1$), and one HC_bC_bH torsion (A_2). In addition, the C_bHC_bH bridge is associated with three hindered rotational

TABLE 1: Experimental and Calculated (DF/B3LYP Results, 6-31G and cc-pVDZ Basis Sets) C−C Distances (Å) of 4, 5, 2, and 6 (see Figure 1)**

	4			**5**			**2**			**6**		
	B3LYP/ 6-31G**	B3LYP/ cc-pVDZ	expt[b]	B3LYP/ 6-31G**	B3LYP/ cc-pVDZ	expt[c]	B3LYP/ 6-31G**	B3LYP/ cc-pVDZ	expt[d]	B3LYP/ 6-31G**	B3LYP/ cc-pVDZ	expt[e]
$R_{1,2}$[a]	1.399	1.402	1.406	1.413	1.415	1.413	1.419	1.421	1.412	1.430	1.432	1.437
$R_{2,3}$[a]	1.395	1.397	1.381	1.389	1.391	1.387	1.389	1.391	1.370	1.370	1.372	1.397
$R_{3,4}$[a]	1.413	1.415	1.404	1.423	1.425	1.414	1.426	1.428	1.402	1.426	1.428	1.422
$R_{6,7}$[a]	1.400	1.403	1.387	1.402	1.404	1.395	1.404	1.406	1.393	1.401	1.403	1.392
$R_{1,6}$[a,f]	2.513	2.514	2.469	2.408	2.408	2.384	2.400	2.402	2.410	1.445	1.447	1.437
$R_{1,15}$[a]	1.517	1.518	1.524	1.515	1.516	1.517	1.511	1.512	1.498			
$R_{15,16}$[a]	1.548	1.548	1.570	1.523	1.523	1.518	2.933	2.933	2.917			
$R_{15,17}$[a]				2.444	2.444	2.434						
H···H[g]							1.699	1.686	1.780			
A[h]	0.996	0.996	0.986	0.984	0.984	0.984	0.978	0.978	0.969	0.932	0.932	0.958
Δr_m[i]	0.013	0.013	0.012	0.019	0.019	0.014	0.019	0.019	0.023	0.034	0.034	.027

[a] Atom pairs as in Figure 1. [b] Structural data on the annulene ring of the 15,16-dimethyl derivative of **4** taken from ref 30. [c] From ref 16. [d] From ref 15. [e] From ref 33. [f] In the case of **4**, **5** and **2** the distance is between nonbonded C atoms. [g] The closest distance between nonbonded hydrogens of the two CH_2 bridge groups. [h] Julg parameter (see text for definition). [i] Maximum deviation of the C−C bondlength (Å) along the ring from the mean value.

motions (R_x, R_y, R_z, classified as wagging (B_2), rocking (B_1), and twisting (A_2), respectively) and three hindered translations (T_x (B_1), T_y (B_2), T_z (A_1), approximately described by stretching CC_b and bending CC_bC coordinates modes of the two bridges $C_1C_bC_6$ and $C_8C_bC_{13}$). In the more complicated case of **5**, the bridge modes (21) are classified as $7A_1 + 3A_2 + 6B_1 + 5B_2$. With the C_{15} and C_{17} atoms as C_b, they may be represented to a good approximation as linear combinations of C_bH stretchings (2), $C_{16}H$ stretchings (2), C_bC_{16} stretchings (2), $C_bC_{16}C_b$ bending (1), $HC_{16}H$ bending (1), $C_{16}H_2$ wagging, rocking, and twisting (3), $C_{16}C_bH$ bendings (2), out-of-plane $C_bC_{16}C_bH$ bendings (2), and finally as hindered rotations and translations of the $C_bHC_{16}H_2C_bH$ fragment (6). In the same approximation, the remaining 66 normal modes of both systems are substantially localized on the ring, having the anthracene perimeter and the same number of atoms. A correspondence may thus be attempted between the normal modes of anthracene (D_{2h} symmetry) and the ring modes of **4** and **5** (C_{2v} symmetry), according to the correlation $[A_g, B_{1u}] \rightarrow A_1$, $[B_{1g}, A_u] \rightarrow A_2$, $[B_{2g}, B_{3u}] \rightarrow B_1$, $[B_{3g}, B_{2u}] \rightarrow B_2$.

The frequencies of **4** and **5** in their optimized ground-state structure have been calculated with the cc-pVDZ basis set and the B3LYP functional. The normal-mode analysis of **4** confirms that the partitioning into ring and bridge modes is substantially reasonable. Accordingly, the frequencies have been reported separately in Tables 2 and 3. For correlation purposes, cc-pVDZ/B3LYP vibrational data on anthracene have also been obtained, in full agreement with previous data.[23] Calculations based on the 6-31G** basis set give nearly identical normal mode displacements, while vibrational frequencies mostly shifted to higher values (∼1−5 cm^{-1} below 1000 cm^{-1}, ∼3−25 cm^{-1} above 1000 cm^{-1}). If we neglect from now on the C−H stretching modes from our discussion and focus the attention on bridge modes, the C_bC_b vibration of **4** is found at 1028 cm^{-1}, the two bendings at 1231 and 1245 cm^{-1}, and the HC_bC_bH torsion at 1264 cm^{-1}. The rocking, twisting, and wagging modes fall at 914 (R_y), 984 (R_z), and 1253 (R_x) cm^{-1} and the hindered translations at 791 (T_x), 849 (T_z), and 974 (T_y) cm^{-1}. These latter and the rocking mode are coupled with ring coordinates.

As to **5**, several bridge modes may be easily identified. For instance, the 1025 and 1097 cm^{-1} vibrations are the symmetric and antisymmetric C_bC_{16} stretching motions, while those at 1299 and 1259 cm^{-1} are the two corresponding $C_{16}C_bH$ bendings. In other cases (mostly involving hindered rotational and translational motions of the $C_bHCH_2C_bH$ group), the so-called bridge modes of **5** have contributions from ring coordinates so that this schematic assignment appears less plausible, though still useful for descriptive purposes. For the sake of comparison, the well-localized bridge modes of 1,6-methano[10]annulene (cc-pVDZ/B3LYP) have been added to those of **4** and **5** in Table 3. All other calculated vibrations of **4** and **5** below 1700 cm^{-1} have been correlated with those of anthracene on the basis of the previous symmetry considerations and of the actual vibrational eigenvectors in Table 2.

B. Vibrational Spectra. Infrared and Raman data of **4** and **5**, taken at room temperature, are reported in Figures 2−5. In the far-infrared region (200−500 cm^{-1}; Figure 2), both spectra have low absorbance. In contrast, the mid-infrared region shows bands of medium/strong intensity (604, 689, 739, 887, 900, and 916 cm^{-1} for **4**; 615, 699, and 908 cm^{-1} for **5**; Figure 3) in the same range (∼600−900 cm^{-1}) where the strongest infrared bands of anthracene are found.[36] The Raman spectra of **4** and **5** (λ_{exc} = 1064 nm) have several intense peaks between 200 and 600 cm^{-1} (124, 228, 413, and 602 cm^{-1} for **4**; 138, 251, 420, and 615 cm^{-1} for **5**; Figures 4 and 5, respectively), at variance with anthracene of which the strongest Raman lines occur in the upper 1100−1600 cm^{-1} region.[26,36] As to **4**, Raman lines of medium intensity are observed at 959, 1478, 1482, and 1555 cm^{-1}. The infrared and Raman activity increases with respect to that of anthracene mainly because of disappearance of the inversion center in the molecular symmetry. As a result, a large number of medium/weak bands may be observed in the two spectra. A second, less important, reason for such an abundance is related to solid-state effects. Because the crystal structure of **4** is not known, our considerations are solely based on the crystal structure of **5**.[16] First, the reduced site symmetry (C_1) imposes that molecular modes of any symmetry are infrared active. Molecular modes of A_2 symmetry are however expected to show weakly in the infrared spectrum of the crystal. Accordingly, the weak infrared bands at 1164 and 1198 cm^{-1}, having strong Raman counterparts, have been assigned to A_2 modes. Second, each molecular mode splits into four crystal components, $A_1 + A_2 + B_1 + B_2$, all of them Raman and only three, except A_2, infrared active. Experimentally, most infrared and Raman bands are single and coincident within ∼1−3 cm^{-1}. No infrared triplets or Raman quartets are observed. The two infrared doublets, 570/575 cm^{-1} and 1211/1214 cm^{-1}, are assigned as pairs of crystal components. Also, some intense bands of both spectra have shoulders, which may be part of

TABLE 2: Calculated Ring Frequencies (cm^{-1}; DF/B3LYP Results, cc-pVDZ Basis Set) of 6, 4, and 5 (see Figure 1) Using Scaling Factors 0.983 for In-plane Bendings and 0.970 for the Remaining Vibrations, as Recommended in Ref 23[a]

6			**4**			**5**		
raw	scaled	approximate description	raw	scaled	approximate description	raw	scaled	approximate description
A_g			A_1			A_1		
398	391	CC_tC	422	415		431	424	
638	627	CCC_t; C_tCC_t				587	577	
			704	692	CCCH	711	689	
765	742	C_tC_t	613	594	$C_tC_bC_t$	628	610	$C_tC_bC_t$
1034	1003	*o*-CCH; *o*-CC	988	959	$+C_bC_b$	1000	970	$+C_bC_{16}C_b$
1177	1157	*o*-CCH	1248	1227	$+C_bC_bH$	1232	1211	*o*-CCH
1294	1272	*o*-CCH; *i*-CC	1361	1337	$+C_bC_bH$	1368	1324	$+C_{16}C_bH$
1445	1402	*o*-CC; C_tC_t	1393	1351	*o*-CC; C_bC_t	1419	1376	C_bC_t; $C_{16}C_bH$
1517	1472	*o*-CCH; C_tC; *o*-CC	1608	1560		1556	1510	
1604	1555	CC; C_tC_t; *o*-CCH	1547	1501	*o*-CC; *o*-CCH	1533	1487	*o*-CC; *o*-CCH
B_{1u}								
94	90	butterfly	102	99		121	118	
390	379	CCCC	394	382		393	381	
485	470	CCCC; CC_tCH; C_tC_tCH	239	232	$+C_tC_bC_t$	258	250	$+C_tC_bC_t$
749	726	CCCH; CC_tCH; C_tC_tCH	753	730		777	754	
908	881	CCCH; C_tC_tCH	909	882		908	881	
981	951	CCCH; CC_tCH; C_tC_tCH	944	915		940	912	
B_{1g}			A_2			A_2		
395	388	CC_tC	489	481	$+R_z$ (bridge)	415	408	$+R_z$ (bridge)
533	524	*o*-CCC	372	366		348	342	$+R_z$ (C_bH_2)
924	908	CCC	887	872		908	893	$+R_z$ (bridge)
1125	1106	*o*-CCH; *i*-C_tCH	1135	1116		1138	1118	
1199	1180	*o*-CCH; *i*-C_tCH	1190	1170		1217	1196	$+R_z$ (bridge)
1281	1259	*o*-CCH; *i*-C_tC_tC	1348	1325	$+C_tC_b$; *i*-C_tCH	1355	1332	$+C_tC_b$; *i*-C_tCH
1404	1380	*o*-CCH	1423	1399		1425	1400	
1631	1582	*o*-CC; *i*-C_tC; *o*-CCH; *i*-C_tCH	1542	1496		1566	1519	
1679	1628	*o*-CC; *i*-C_tC; *o*-CCH; *i*-C_tCH	1607	1559		1604	1556	
A_u								
123	119	ring torsion	107	104		114	111	
512	497	CCCC	460	446		493	484	
774	750	CC_tCH; CCCC	627	608		635	616	
881	854	CCCH; CC_tCH	853	827		841	816	
1004	974	CCCH; CC_tCH	994	964		986	956	
B_{3u}			B_1			B_1		
614	604	CCC_t	367	360	$+R_y$ (bridge)	336	330	$+R_y$ (bridge)
825	800	C_tC_t; *o*-C_tC	669	649	$C_tC_bC_t$	604	585	$C_tC_bC_t$
1030	999	*o*-CCH; *o*-CC	979	950	$+i$-C_tCH	974	945	$+i$-C_tCH
1155	1135	*o*-CCH; *i*-C_tCH	1127	1108		1142	1122	
1182	1162	*o*-CCH; *i*-C_tCH	1221	1200		1219	1199	
1386	1345	*o*-CC; *i*-C_tC; *o*-CCH; *i*-C_tCH	1332	1292		1374	1333	
1427	1384	*o*-CC; *i*-C_tC; *o*-CCH; *i*-C_tCH	1352	1311	$+C_tC_b$	1391	1349	$+C_tC_b$; $C_{16}C_bH$
1477	1452	*o*-CC; *o*-CCH	1467	1442	$+i$-C_tC; *i*-C_tCH	1473	1448	$+i$-C_tC; *i*-C_tCH
1587	1540	*o*-CC; *i*-C_tC; *o*-CCH; *i*-C_tCH	1597	1549		1580	1533	
B_{2g}								
239	232	ring torsion	220	213		222	215	
491	476	CC_tCH; CCCC	501	486		445	432	
777	754	CCCH; CC_tCH	743	721		687	666	
976	947	CCCH; CC_tCH	884	858		883	857	
B_{2u}			B_2			B_2		
235	231	CC_tC	262	258		265	260	
659	648	*o*-CCC; *o*-C_tC_tC	572	562		582	572	
913	897	*o*-CCC; C_tCC_t	876	861		876	862	
1165	1145	*o*-CCH	1175	1155		1170	1150	
1281	1259	*o*-CCH; C_tCC_t	1368	1344	$+C_tC_b$	1377	1354	$+C_tC_b$
1338	1298	*o*-CCH; *i*-C_tC	1341	1301		1334	1294	$+C_tC_bH$
1486	1442	*o*-CCH; C_tC	1501	1456		1482	1438	
1679	1629	*o*-CC; *o*-C_tC; *o*-CCH	1652	1603		1629	1580	
B_{3g}								
273	265	ring torsion	235	228		230	223	
594	576	CCCC	520	504		529	513	
796	772	CC_tCH; C_tC_tCH	629	610		639	620	
858	832	CCCH; CC_tCH; C_tC_tCH	837	812		823	798	
932	904	CCCH; CC_tCH; C_tC_tCH	921	894		933	905	
1004	974	CCCH; CC_tCH	993	964		988	958	

[a] Ring modes are approximately represented by two, three, and four letter groups, corresponding to stretchings, in-plane bendings, and out-of-plane bendings + torsions, respectively. Symbols are as follows: C_t, transannular, that is, 1, 6, 8, and 13, C Atoms; C_b, bridge atoms, that is, 15 and 16 in **4** and 15 and 17 in **5**; *o* and *i*, prefixes for displacements localized on the C atoms belonging to the two external (outer) rings of **6** and to the central (inner) ring; bridge, C_bHC_bH in **4** and $C_bHCH_2C_bH$ in **5**. Similar modes of **6**, **4**, and **5** are described only under the **6** heading; additional internal coordinates of **4** and **5** follow the + sign.

TABLE 3: Correlation between Calculated Bridge Frequencies (cm^{-1}; DF/B3LYP Results, cc-pVDZ Basis Set) of 1, 4, and 5 (see Figure 1) Using the Scaling Factor 0.970[a]

1		4		5		approximate description
raw	scaled	raw	scaled	raw	scaled	
				A_1		
899[b]	872	849[b]	823			T_z (bridge)
				967[b]	938	$C_bC_{16}C_b$
		1028	998			C_bC_b
				1025	994	C_bC_{16}
		1231[b]	1194			C_bC_bH
				1299	1277	$C_{16}C_bH$
1527	1481			1470	1426	$HC_{16}H$
				A_2		
1136	1102	984	954	880[b]	854	R_z (bridge)
				1183	1148	$C_bC_{16}C_bH$; R_z ($C_{16}H_2$)
		1264	1226			HC_bC_bH
				1291	1252	$C_bC_{16}C_bH$; R_z ($C_{16}H_2$)
				B_1		
442	429	791[b]	767	768[b]	745	T_x (bridge)
		914[b]	886	854[b]	828	R_y (bridge)
1049	1018					R_y (bridge)
				1097	1064	C_bC_{16}
		1245	1208			C_bC_bH
				1259	1221	$C_{16}C_bH$
				1339[b]	1299	$C_{16}C_bH$; R_y ($C_{16}H_2$); C_bC_{16}
				B_2		
				385	373	T_y ($C_{16}H_2$)
				827[b]	802	R_x ($C_{16}H_2$)
956[b]	928	974[b]	945			T_y (bridge)
1314	1275	1253	1215	1061	1029	R_x (bridge)
				1258	1220	$C_bC_{16}C_bH$

[a] Bridge modes are approximately represented by two, three, and four letter groups, corresponding to stretchings, in-plane bendings, and out-of-plane bendings + torsions, respectively. Symbols are as follows: C_b, bridge C atoms, that is, 15 and 16 in **4** and 15 and 17 in **5**; bridge, CH_2 in **1**, C_bHC_bH in **4**, and $C_bHC_{16}H_2C_bH$ in **5**. [b] Modes appreciably mixed with ring displacements.

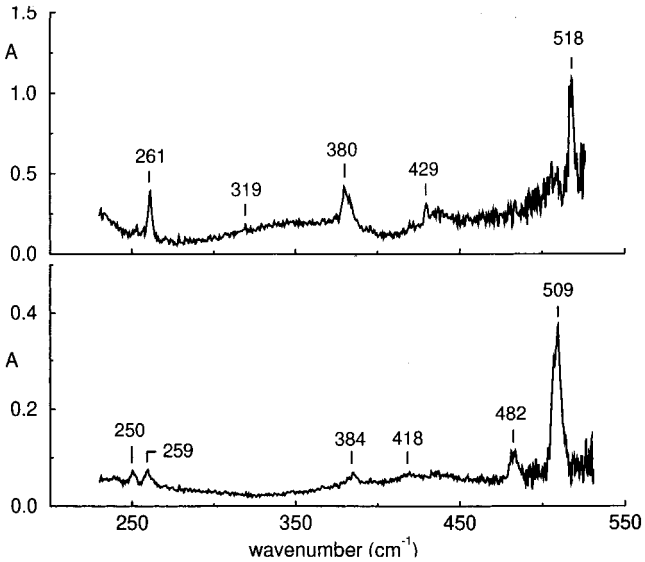

Figure 2. Infrared spectra of **4** (lower) and **5** (upper) as polycrystalline films between CsI windows at room temperature in the range 230−520 cm^{-1}.

unresolved crystal multiplets. Finally, hot band structure, that is, transitions from upper vibrational levels of low-frequency torsional modes, and bands due to isotopic impurities, particularly those containing ^{13}C, may further enrich the vibrational spectra of **4** and **5**. Because the assignment and the characterization of fundamental modes is the main concern of the present paper, the latter weak resonances have been excluded from the vibrational analysis of the next section.

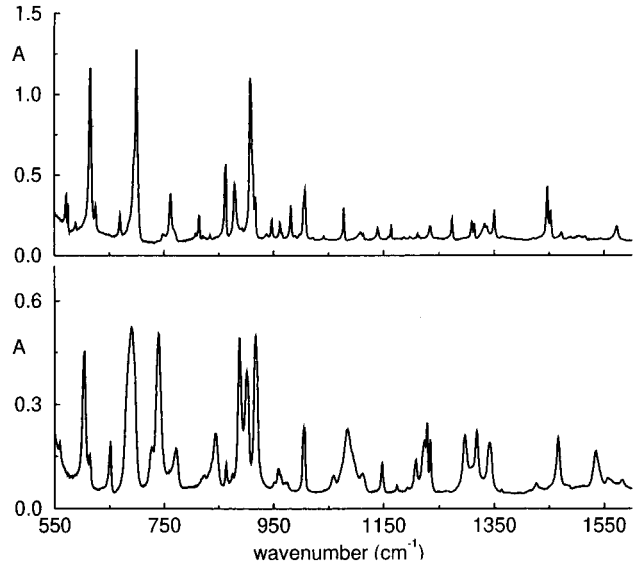

Figure 3. Infrared spectra of **4** (lower) and **5** (upper) as polycrystalline films between CsI windows at room temperature in the range 550−1600 cm^{-1}.

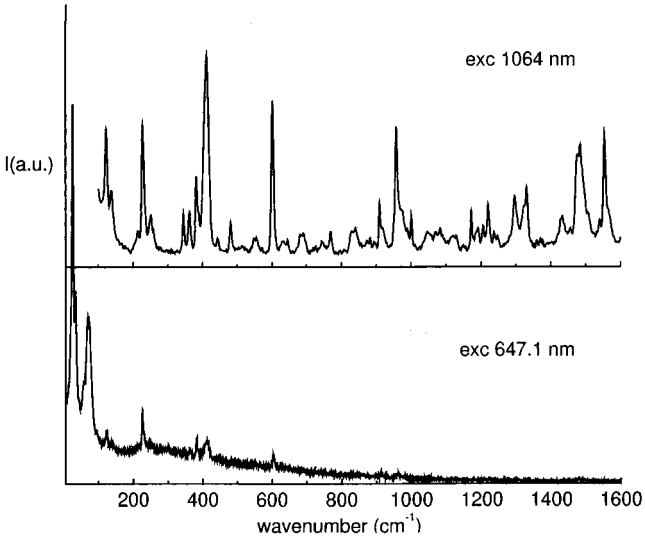

Figure 4. Raman spectra of polycrystalline **4** at room temperature for two excitation wavelengths, 1064 (upper) and 647.1 nm (lower).

With excitation at 647.1 nm, the Raman peaks of **4** between 100 and 600 cm^{-1} are strongly depressed and those above 1000 cm^{-1} disappear completely, while a diffuse background intensity underlies the Raman emission (Figure 4). The relative intensity of the observed bands, 228, 413, and 602 cm^{-1}, changes as a result of the excitation wavelength shift to 647.1 nm. The combination of two factors may contribute to the observed behavior, namely, (i) a preresonance effect as λ_{exc} approaches the lowest electronic transition and (ii) because **4** is fluorescent[20] a weak fluorescence emission activated by the small absorption of **4** as crystalline powder exciting at 647.1 nm. The second factor does not play any role for **5** because the lowest $\pi\pi^*$ transition of **5** is at energy higher than that of **4** and has a lower oscillator strength.[20] As a consequence, in the spectrum of **5**, the preresonance enhancement of the 251 cm^{-1} peak may be better appreciated (Figure 5).

As a last comment, it should be noted that also the Raman lattice modes of **4** and **5** have been measured at 647.1 nm

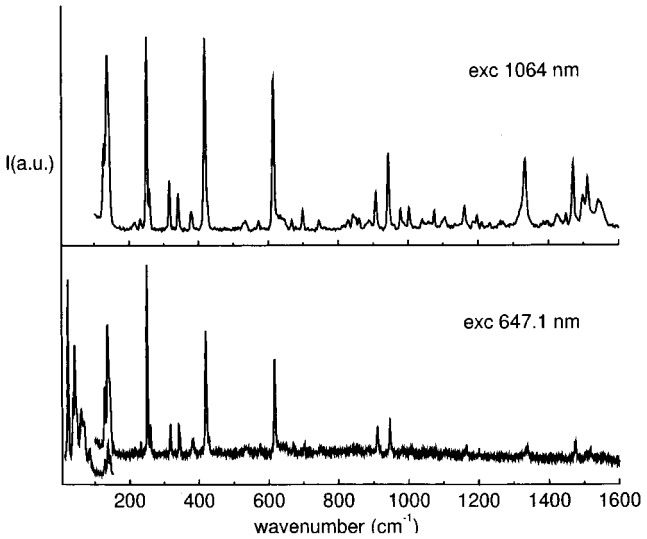

Figure 5. Raman spectra of polycrystalline **5** at room temperature for two excitation wavelengths, 1064 (upper) and 647.1 nm (lower).

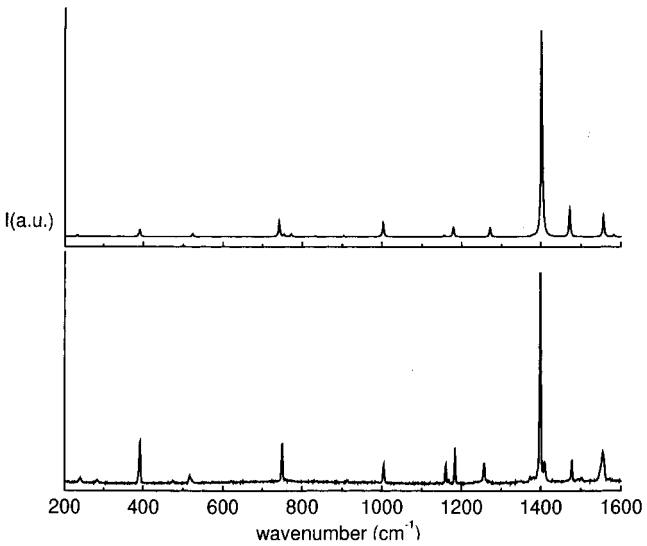

Figure 6. Experimental (lower) and calculated (upper; DF/B3LYP, cc-pVDZ basis set) Raman spectrum of anthracene. Experimental spectrum was taken with anthracene as a polycrystalline sample at room temperature. Calculated spectrum was generated with Lorentzian full bandwidth, 2Γ, equal to 4 cm^{-1}. The relative intensities on the vertical axis are scaled such that the strongest peaks match in appearance.

(Figures 4 and 5, respectively). Seven peaks are observed for **5** (23, 36, 42, 47, 59, 68, and 83 cm^{-1}), much less than the expected number (21), and five for **4** (25, 34, 57, 71, and 93 cm^{-1}). Given the differences in the number of lattice modes, their frequencies, and spectral pattern, the crystal structures of **4** and **5**, directly responsible of the observed Raman spectrum in the lattice region, must be noticeably different.

IV. Discussion

The vibrational properties of several polycyclic aromatic hydrocarbons (including anthracene) have been theoretically treated by DF calculation methods.[23] It was shown that calculated frequencies with the B3LYP exchange−correlation functional[28,29] and the cc-pVDZ basis set fit accurately the experimental values provided that a scaling factor of 0.983 is used for in-plane bendings and a second, 0.970, for the remaining modes (except C−H stretchings). During this work, in addition to frequencies, Raman intensities of anthracene have been calculated. The satisfactory agreement with experiment, as shown in Figure 6, invites the use of calculated Raman intensities also for the vibrational assignment of **4** and **5**. Observed and scaled frequencies and corresponding infrared and Raman strengths (B3LYP/cc-pVDZ) of **4** and **5** and anthracene are reported in Table 4. The scaling factors of anthracene[23] have been transferred to the modes of the [14]annulenes **4** and **5** reported in Table 2, while all of the bridge modes included in Table 3 have been uniformly scaled by 0.970. On the whole, the average rms deviation between observed and calculated values is ≤ 15 cm^{-1} for both molecules. Experimental and calculated spectra of Figures 7 and 8 give the visual estimate of the good agreement between the two sets of data. In the following, we will shortly comment the prominent features of the assignment summarized in Table 4.

A. Bridge Modes. All bridge modes of **4** arising from internal degrees of freedom of the C_bHC_bH fragment, though relatively weak, may be identified in the infrared and Raman spectra. The C_b-C_b stretching mode, calculated at 998 cm^{-1}, is observed at 1004/1 (IR/R) cm^{-1}; C_bC_bH bending modes occur at near frequencies (sym, A_1, obsd 1207/6 (IR/R), calcd 1194 cm^{-1}; antisym, B_1, obsd 1223/28/20 (IR/IR/R), calcd 1208 cm^{-1}), the latter having an intensity larger than the former; the weak torsional mode HC_bC_bH (A_2) has been located at 1247 cm^{-1} in the Raman spectrum (1226 cm^{-1}, calcd). Among hindered rotational and translational modes of the bridge, T_x (B_1) and T_z (A_1) give relatively weak absorptions at 772/70 (IR/R) and at 844/2 cm^{-1} (IR/R), in agreement with calculations. All other modes are either not observed [R_z (A_2), calcd 954 cm^{-1}; R_x (B_2), calcd 1215 cm^{-1}] or weak [R_y (B_1), obsd 875/4 cm^{-1} (IR/R), calcd 886 cm^{-1}; T_y (B_2), obsd 962 cm^{-1} (IR/R), calcd 945 cm^{-1}]. In the last case, the assignment should therefore be regarded as tentative.

As to **5**, the strongest bridge modes occur at 944 cm^{-1} in the Raman (947 cm^{-1}, IR, weak) and at 1007 cm^{-1} in the infrared spectrum (1004 cm^{-1}, R, weak). These are assigned to the $C_bC_{16}C_b$ bending and to the symmetric C_bC_{16} stretching, respectively. Other relatively strong infrared or Raman bands or both are the symmetric $C_{16}C_bH$ bending (1274/2 cm^{-1}, IR/R), the $HC_{16}H$ bending (1452/1 cm^{-1}, IR/R), the symmetric $C_bC_{16}C_bH$ out-of-phase (oop) bending (1164/2 cm^{-1}, IR/R), the antisymmetric C_bC_{16} stretching (1077/5 cm^{-1}, IR/R), and the antisymmetric $C_bC_{16}C_bH$ oop bending (1234 cm^{-1}, IR). Hindered translational and rotational modes are less intense in both spectra and have been only tentatively assigned in Table 4 (747 cm^{-1}, IR and R, T_x; 1041 cm^{-1}, IR and R, R_x; 852 cm^{-1}, R, R_y; 813 cm^{-1}, IR, $R_x(C_{16}H_2)$).

B. Ring Modes. The strongest Raman lines of **4** at 228, 413, 602, 959, 1485, and 1555 cm^{-1} are assigned to totally symmetric modes completely or substantially localized on the annulene ring. The lowest three peaks have clear counterparts in the spectrum of **5** at 251, 420, and 615 cm^{-1} and are correlated with anthracene modes at 465 (B_{1u}), 392 (A_g), and 753 (A_g) cm^{-1} (470, 391, and 742 cm^{-1}, calcd), according to the results of Table 4. Denoted as C_t, the transannular, that is, 1, 6, 8, and 13, C atoms, the 742 cm^{-1} mode, represented to a good approximation by anthracene C_tC_t stretching coordinates, is correlated to modes of lower frequency in bridged annulenes, [594 (**4**) and 610 (**5**) cm^{-1}, calcd] as C_tC_t stretchings transform into $C_tC_bC_t$ bendings in the latter systems. On the contrary, although the 470 cm^{-1} mode is an oop Raman inactive mode in anthracene, the coupling of this motion with the bridge $C_tC_bC_t$ bendings of **4** and **5** makes the central ring more planar and dramatically enhances the totally symmetric transient polarization while weakening the frequency mode. It is interesting to

TABLE 4: Observed (expt) Infrared (IR; Polycrystalline Film) and Raman (R; Crystal Powder) Frequencies (cm^{-1}) of Anthracene, 1,6:8,13-Ethane-1,3-diylidene[14]annulene, and 1,6:8,13-Propane-1,3-diylidene[14]annulene (6, 4, and 5 in Figure 1, Respectively) at Room Temperature; Calculated Frequencies, ω (calc, cm^{-1}), Infrared and Raman Intensities (I_{IR} and I_R, respectively, in km mol^{-1} and $Å^4$ amu^{-1}), and Mode Symmetry (sym) Resulting from DF/B3LYP/cc-pVDZ Calculation and Scale Factors from Ref 23 (See Text for Details)[a]

6						4						5					
expt		calcd				expt		calcd				expt		calcd			
IR[b]	R	ω	I_{IR}	I_R	sym	IR	R	ω	I_{IR}	I_R	sym	IR	R	ω	I_{IR}	I_R	sym
105		90	0.93		B_{1u}		138	99	0.1	0.65	A_1		138	118	0.02	8.75	A_1
		119			A_u		124	104		5.14	A_2		128	111		10.31	A_2
	240	232		5.86	B_{2g}		213	213	0.22	1.58	B_1		217	215	0.01	0.66	B_1
	282	265		0.22	B_{3g}	250	251	228	0.39	1.24	B_2		234	223	0.10	3.17	B_2
465		470	16.97		B_{1u}		228	232	1.27	26.62	A_1		251	250	0.01	28.08	A_1
235		231	1.37		B_{2u}	259		258	1.49	1.48	B_2	261	261	260	1.25	2.77	B_2
601		604	8.39		B_{3u}		345	360	0.32	4.43	B_1	319	317	330	0.77	6.29	B_1
	516	524		11.50	B_{1g}		363	366		9.83	A_2		343	342		6.54	A_2
														373	0.87	1.46	B_2
391		379	0.02		B_{1u}	384	383/9	382	0.28	13.23	A_1	380	381	381	0.39	7.29	A_1
	392	391		26.65	A_g		413	415	0.18	54.08	A_1		420	424	0.19	52.48	A_1
		497			A_u		444	446		3.87	A_2			484		2.87	A_2
	391	388		4.22	B_{1g}			481		3.57	A_2			408		3×10^{-3}	A_2
	478	476		0.37	B_{2g}	482	482	486	0.05	1.62	B_1	429	429	432	0.05	0.13	B_1
	578	576		0.07	B_{3g}	509		504	11.28	1.61	B_2	518		513	9.67	0.13	B_2
651		648	0.67		B_{2u}	559	549/556	562	0.31	0.56	B_2	570/575	574	572	2.38	0.08	B_2
	622	627		1.38	A_g									577	1.48	1.78	A_1
	753	742		62.78	A_g	604	602	594	10.77	47.03	A_1	615	615	610	15.46	63.93	A_1
		750			A_u			608		0.84	A_2		635	616		0.05	A_2
	775	772		11.08	B_{3g}	613		610	1.46	4.12	B_2	624		620	2.51	1.86	B_2
795		800	0.01		B_{3u}	651	646	649	9.51	3.32	B_1		588	585	0.57	2.65	B_1
						689	682/91	692	38.15	1.52	A_1	699	700	689	61.36	5.95	A_1
	770	754		8.61	B_{2g}		730	721	0.11	4.60	B_1	669	669	666	6.15	11.51	B_1
	770	754		8.61	B_{2g}	772	770	767	9.62	0.40	B_1	747	747	745	1.69	0.89	B_1
725		726	56.0		B_{1u}	739	744	730	34.55	2.41	A_1	761		754	6.31	3.71	A_1
	830	832		2.21	B_{3g}		831	812	0.35	2.73	B_2	834	832	798	1.32	4.57	B_2
												813		802	1.65	1.53	B_2
						844	842	823	0.01	8.38	A_1						
		854			A_u			827		0.22	A_2			816		1.04	A_2
													842	854		1.09	A_2
908		897	1.67		B_{2u}			861	0.04	0.08	B_2	863		862	6.35	0.39	B_2
	956	947		0.54	B_{2g}	863	858	858	10.51	5.31	B_1		862	857	1.2	11.11	B_1
	901	908		0.17	B_{1g}			872		0.32	A_2		890	893		0.08	A_2
877		881	38.15		B_{1u}	887	883	882	20.94	9.58	A_1	879		881	11.05	18.84	A_1
						875	874	886	0.15	0.34	B_1		852	828	1.99	2.08	B_1
	916	904		2.62	B_{3g}	900	899	894	20.73	0.24	B_2	917		905	29.24	2.27	B_2
954		951	4.50		B_{1u}	916	910	915	13.45	23.66	A_1	908	908	912	8.67	23.30	A_1
							920	945	0.23	4.48	B_2						
												947	944	938	1.30	36.80	A_1
996		999	5.85		B_{3u}	973	974	950	0.35	0.40	B_1	962	962	945	0.43	0.03	B_1
		974			A_u			964		0.01	A_2			956		0.01	A_2
	975	974		0.41	B_{3g}		990	964	0.58	0.12	B_2			958	1.88	0.32	B_2
	1007	1003		56.38	A_g		959	959	0.32	65.53	A_1	981	979	970	3.83	21.54	A_1
								954		0.03	A_2						
						1004	1001	998	3.03	14.04	A_1						
												1007	1004	994	5.63	18.02	A_1
												1041	1041	1029	0.03	1.27	B_2
												1077	1075	1064	7.60	3.80	B_1
1128		1135	1.52		B_{3u}	1084	1083	1108	38.74	4.74	B_1	1108	1107	1122	15.06	5.41	B_1
	1103	1106		1.15	B_{1g}		1120	1116		4.55	A_2			1118		0.46	A_2
1150		1145	6.30		B_{2u}	1148	1149	1155	0.63	0.14	B_2	1140	1137	1150	1.15	0.61	B_2
												1164	1162	1148		18.88	A_2
	1186	1180		36.58	B_{1g}		1172	1170		21.46	A_2	1198	1198	1196		8.93	A_2
1165		1162	2.19		B_{3u}	1193	1191	1200	0.77	5.77	B_1	1186	1187	1199	0.17	4.72	B_1
						1207	1206	1194	0.43	4.65	A_1	1274	1272	1277	1.08	3.42	A_1
	1163	1157		6.42	A_g	1234	1237	1227	0.65	4.70	A_1	1211/14	1212	1211	0.09	0.48	A_1
						1223/28	1220	1208	10.02	8.10	B_1		1235	1221	0.23	4.44	B_1
								1215	2.52	1.61	B_2	1234		1220	2.63	0.22	B_2
							1247	1226		5.64	A_2						
														1252		0.90	A_2
														1299	1.24	1.92	B_1
1342		1345	3.27		B_{3u}	1296	1297	1292	12.39	22.68	B_1	1333	1334	1333	2.76	40.26	B_1
1316		1298	6.03		B_{2u}		1324	1301		0.01	B_2	1314		1294	1.05	0.04	B_2
	1274	1259		0.048	B_{1g}			1325		0.16	A_2			1332		0.14	A_2
1397		1384	1.61		B_{3u}	1318		1311	2.91	0.10	B_1			1349	1.18	2.30	B_1
1271		1259	5.49		B_{2u}	1341		1344	10.69	0.02	B_2	1350		1354	5.86	0.56	B_2

TABLE 4 (Continued)

6						**4**						**5**					
expt		calcd				expt		calcd				expt		calcd			
IR[b]	R	ω	I_{IR}	I_R	sym	IR	R	ω	I_{IR}	I_R	sym	IR	R	ω	I_{IR}	I_R	sym
	1260	1272		38.29	A_g		1331	1337	0.01	58.56	A_1	1336	1334	1324	0.26	57.17	A_1
	1400	1402		812.55	A_g		1360	1351	0.21	0.79	A_1		1403	1376	0.11	1.80	A_1
	1374	1380		3.70	B_{1g}	1426	1433	1399		5.19	A_2		1426	1400		9.81	A_2
1476		1452	1.45		B_{3u}		1457	1442	0.47	2.65	B_1		1451	1448	0.02	9.97	B_1
1450		1442	1.42		B_{2u}	1465		1456	5.86	0.07	B_2	1446		1438	2.53	0.96	B_2
												1452	1451	1426	2.76	11.50	A_1
	1556	1555		83.11	A_g	1485	1485	1501	0.62	86.68	A_1	1472	1472	1487	1.84	74.93	A_1
	1574	1582		7.37	B_{1g}		1478	1496		42.89	A_2		1500	1519		14.87	A_2
1540		1540	5.31		B_{3u}	1534		1549	10.96	0.32	B_1	1514		1533	6.96	2×10^{-3}	B_1
	1627	1628		2.77	B_{1g}	1542		1559		0.02	A_2		1544	1556		1.59	A_2
	1480	1472		106.0	A_g	1556	1555	1560	0.24	55.20	A_1		1513	1510	0.42	115.56	A_1
1626		1629	5.60		B_{2u}	1582		1603	0.01	1.64	B_2	1573		1580	1.80	1.40	B_2

[a] C−H stretching frequencies are not reported in the table. [b] From ref 25 and references therein.

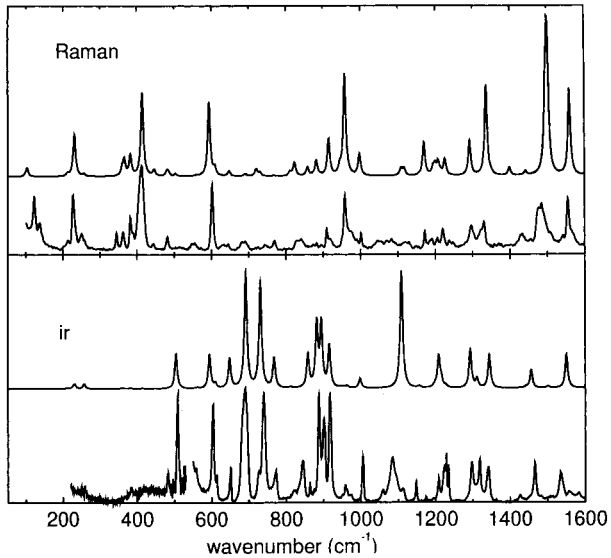

Figure 7. Experimental and calculated (DF/B3LYP, cc-pVDZ basis set) vibrational spectra of **4**: (lower) infrared (IR) spectrum; (upper) Raman spectrum with $\lambda_{exc} = 1064$ nm. Calculated spectra (second and fourth trace from the bottom) were generated with Lorentzian full bandwidth, 2Γ, equal to 8 cm^{-1}. Relative Raman intensities on the vertical axis are scaled such that the 602 cm^{-1} (exptl) and the 594 cm^{-1} (calcd) band intensities are equal. Relative infrared intensities on the vertical axis are scaled such that the 739 cm^{-1} (exptl) and the 730 cm^{-1} (calcd) band intensities are equal.

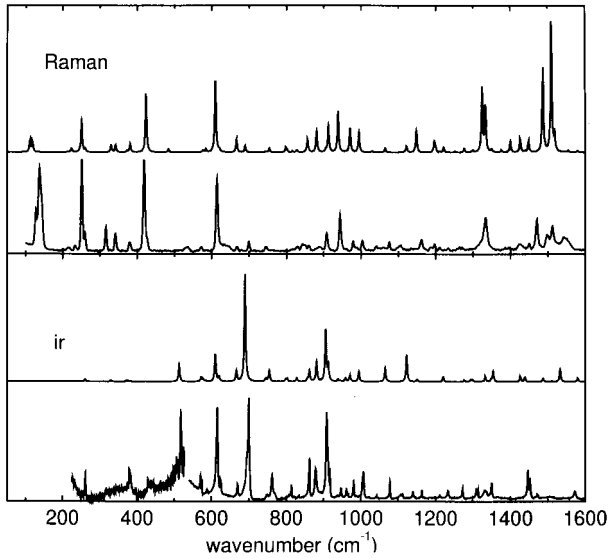

Figure 8. Experimental and calculated (DF/B3LYP, cc-pVDZ basis set) vibrational spectra of **5**: (lower) infrared (IR) spectrum; (upper) Raman spectrum with $\lambda_{exc} = 1064$ nm. Calculated spectra (second and fourth trace from the bottom) were generated with Lorentzian full bandwidth, 2Γ, equal to 4 cm^{-1}. Relative Raman intensities on the vertical axis are scaled such that the 615 cm^{-1} (exptl) and the 610 cm^{-1} (calcd) band intensities are equal. Relative infrared intensities on the vertical axis are scaled such that the 699 cm^{-1} (exptl) and the 689 cm^{-1} (calcd) band intensities are equal.

note that a similar conclusion on the nature of this mode has been reached also from the analysis of the fluorescence spectrum of **4**, in which a large Franck−Condon activity of the 231 cm^{-1} mode has been observed.[19]

From Table 4, it is seen that the 959, 1485, and 1555 cm^{-1} observed peaks of **4** are correlated with those of **5** at 979, 1472, and 1513 cm^{-1} and of anthracene at 1007 (A_g), 1556 (A_g), and 1480 (A_g) cm^{-1}, respectively. The latter two are Raman active modes, both experimentally and from calculations, and retain the intensity in the bridged annulenes. As to the lowest correlation (1007/959/979 cm^{-1}), the small frequency shift agrees with the negligible change of normal coordinate character, which in anthracene is a CCH bending + CC stretching on the outer rings. Their experimental and calculated Raman intensities decrease similarly from anthracene to **5**. There is an opposite frequency shift in the last two cases, that is, 1556/1485/1472 and 1480/1555/1513 cm^{-1} going from anthracene to **4** and to **5**. The former, the in-phase stretching of C_tC_t and front-lying CC bonds in anthracene, becomes more localized on the remote C_3C_4 and $C_{10}C_{11}$ bonds in **4** and **5**. The latter is vice versa a symmetric bending CCH vibration on the outer rings in anthracene, having however additional contributions from C_tC stretchings in **4** and **5**. Apparently, the larger local character of the vibration is associated with the smaller vibrational frequency.

It is at first surprising that no line of **4** or **5** with intensity comparable to that of the 1400 cm^{-1} line of anthracene (1402 cm^{-1}, calcd), by far the strongest spectral feature of Figure 6, can be found in their Raman spectra. When the normal mode is considered, it is easily seen that the atomic displacements of the 1402 cm^{-1} vibration generate a large transient polarizability due to the CC stretching character of the mode. This does not occur in the corresponding normal mode of the [14]annulenes **4** and **5** (1351 and 1376 cm^{-1}, calcd) because the C_tC_t motion is replaced by symmetric C_tC_b stretchings along 1,6 and 8,13 bridges with large displacements of C_t toward C_b atoms. This clearly gives a ring geometry with increased deviation from the nearly planar equilibrium structure of **4** and **5**.

As already noted, intense infrared bands of **4** and **5** occur below 1000 cm^{-1}. For the sake of simplicity, the discussion is limited to these vibrational modes. The correlation between them and with anthracene vibrations is shown in Table 4. Only the pair of strong oop bands, 689 (A_1, **4**) and 699 (A_1, **5**) cm^{-1}, cannot be related to anthracene modes. In all other cases, the correlation (**6**/**4**/**5**) follows without difficulty considering our calculation and the infrared spectra: 578(B_{3g})/509(B_2)/518(B_2) cm^{-1}; 753(A_g)/602(A_1)/615(A_1) cm^{-1}; 725(B_{1u})/739(A_1)/761(A_1) cm^{-1}; 877(B_{1u})/887(A_1)/879(A_1) cm^{-1}; 916(B_{3g})/900(B_2)/917(B_2) cm^{-1}; 954(B_{1u})/916(A_1)/908(A_1) cm^{-1}. Apart from the second triplet, already analyzed, the modes of the [14]annulenes **4** and **5** correlate with oop vibrations of anthracene and are quite similar in shape to those of the parent molecule. As a consequence, the frequency shifts with respect to anthracene are modest. It should be noted that B_{3g} modes of anthracene, inactive in the infrared, are correlated with **4** and **5** modes with strong infrared activity. In these cases, the intensity contributions come from the two oop CCC−H bendings of the central unit, which give rise to B_2 vibrations with large transition dipoles along *y* due to the large out-of-phase CCC−H oscillations.

V. Conclusions

In this paper, we have reported on the infrared and Raman spectra of two representative bridged [14]annulenes with an anthracene perimeter, 1,6:8,13-ethane-1,3-diylidene[14]annulene (**4**) and 1,6:8,13-propane-1,3-diylidene[14]annulene (**5**), and proposed the vibrational assignment on the basis of DF/B3LYP/cc-pVDZ calculations of vibrational frequencies and infrared and Raman intensities.

The great majority of the vibrational modes may be classified as bridge or ring modes according to their atomic displacements to a high degree of confidence, thus allowing a correlation of ring modes of **4** and **5** with modes of anthracene. This supports the aromatic nature of the two molecules, in agreement with structural calculations. Because of the reduced symmetry with respect to anthracene, ring modes may be, in principle, active in both spectroscopies. On the whole, this study, together with the previous report on bridged [10]annulenes,[22] indicates that density functional calculations may be reliably applied to aromatic systems of medium/large size and give substantial help for an accurate analysis of their vibrational properties.

Acknowledgment. This work was supported by the Italian Consiglio Nazionale delle Ricerche (CNR) and Ministero dell′Università e della Ricerca Scientifica e Tecnologica (MURST). The authors wish to thank Prof. C. Taliani and Dr. G. Ruani from Laboratorio di Spettroscopia Molecolare (CNR, Bologna, Italy) for the use of the Raman facility and precious assistance during the measurements. The allocation of computer time from CINECA (Bologna, Italy) is also gratefully acknowledged.

References and Notes

(1) Garratt, P. *Aromaticity*; John Wiley and Sons: New York, 1986.

(2) Minkin, V. I.; Glukhovtsev, M. N.; Simkin, B. Y. *Aromaticity and Antiaromaticity*; John Wiley and Sons: New York, 1994.

(3) Sondheimer, F.; Calder, I. C.; Elix, J. A.; Gaoni, Y.; Garratt, P. J.; Grohmann, K.; Maio, G. D.; Mayer, J.; Sargent, M. V.; Wolovsky, R. *R. Chem. Soc. Spec. Publ.* **1967**, *21*, 75−107.

(4) Boekelheide, V. *Proc. Robert A. Welch Found. Conf. Chem. Res.* **1968**, *12*, 83−121.

(5) Vogel, E. *Proc. Robert A. Welch Found. Conf. Chem. Res.* **1968**, *12*, 215−251.

(6) Müllen, K. *Pure Appl. Chem.* **1986**, *58*, 177−186.

(7) Masamune, S.; Hojo, K.; Hojo, K.; Bigam, G.; Rabenstein, D. L. *J. Am. Chem. Soc.* **1971**, *93*, 4966−4968.

(8) Vogel, E.; Roth, H. D. *Angew. Chem., Int. Ed. Engl.* **1964**, *3*, 228−229.

(9) Vogel, E.; Haberland, U.; Gunther, H. *Angew. Chem., Int. Ed. Engl.* **1970**, *9*, 513−514.

(10) Vogel, E.; Sombroek, J.; Wagemann, W. *Angew. Chem., Int. Ed. Engl.* **1975**, *14*, 564−565.

(11) Vogel, E.; Reel, H. *J. Am. Chem. Soc.* **1972**, *94*, 4388−4389.

(12) Vogel, E.; Vogel, A.; Kübbeler, H. K.; Sturm, W. *Angew. Chem., Int. Ed. Engl.* **1970**, *9*, 514−516.

(13) Bianchi, R.; Pilati, T.; Simonetta, M. *Acta Crystallogr.* **1980**, *B36*, 3146−3148.

(14) Bailey, N. A.; Mason, R. *Chem. Commun.* **1967**, 1039−1040.

(15) Destro, R.; Pilati, T.; Simonetta, M. *Acta Crystallogr.* **1977**, *B33*, 940−942.

(16) Gavezzotti, A.; Mugnoli, A.; Raimondi, M.; Simonetta, M. *J. Chem. Soc., Perkin Trans. II* **1972**, 425−431.

(17) Klingensmith, K. A.; Puttmann, W.; Vogel, E.; Michl, J. *J. Am. Chem. Soc.* **1983**, *105*, 3375−3380.

(18) Dewey, H. J.; Deger, H.; Frolich, W.; Dick, B.; Klingensmith, K. A.; Hohlneicher, G.; Vogel, E.; Michl, J. *J. Am. Chem. Soc.* **1980**, *102*, 6412−6417.

(19) Klingensmith, K. A.; Dewey, H. J.; Vogel, E.; Michl, J. *J. Am. Chem. Soc.* **1989**, *111*, 1539−1546.

(20) Kolc, J.; Michl, J.; Vogel, E. *J. Am. Chem. Soc.* **1976**, *98*, 3935−3948.

(21) Catani, L.; Gellini, C.; Salvi, P. R. *J. Phys. Chem. A* **1998**, *102*, 1945−1953.

(22) Gellini, C.; Salvi, P. R.; Vogel, E. *J. Phys. Chem. A* **2000**, *104*, 3110−3116.

(23) Martin, J. M. L.; El-Yazal, J.; Francois, J.-P. *J. Phys. Chem.* **1996**, *100*, 15358−15367.

(24) Langhoff, S. R. *J. Phys. Chem.* **1996**, *100*, 2819−2841.

(25) Cane′, E.; Miani, A.; Palmieri, P.; Tarroni, R.; Trombetti, A. *J. Chem. Phys.* **1997**, *106*, 9004−9012.

(26) Jas, G. S.; Wan, C.; Kuczera, K.; Johnson, C. K. *J. Phys. Chem.* **1996**, *100*, 11857−11862.

(27) Frisch, M. J.; Trucks, G. W.; Schlegel, H. B.; Scuseria, G. E.; Robb, M. A.; Cheeseman, J. R.; Zakrzewski, V. G.; Montgomery, J. A., Jr.; Stratmann, R. E.; Burant, J. C.; Dapprich, S.; Millam, J. M.; Daniels, A. D.; Kudin, K. N.; Strain, M. C.; Farkas, O.; Tomasi, J.; Barone, V.; Cossi, M.; Cammi, R.; Mennucci, B.; Pomelli, C.; Adamo, C.; Clifford, S.; Ochterski, J.; Petersson, G. A.; Ayala, P. Y.; Cui, Q.; Morokuma, K.; Malick, D. K.; Rabuck, A. D.; Raghavachari, K.; Foresman, J. B.; Cioslowski, J.; Ortiz, J. V.; Stefanov, B. B.; Liu, G.; Liashenko, A.; Piskorz, P.; Komaromi, I.; Gomperts, R.; Martin, R. L.; Fox, D. J.; Keith, T.; Al-Laham, M. A.; Peng, C. Y.; Nanayakkara, A.; Gonzalez, C.; Challacombe, M.; Gill, P. M. W.; Johnson, B. G.; Chen, W.; Wong, M. W.; Andres, J. L.; Head-Gordon, M.; Replogle, E. S.; Pople, J. A. *Gaussian 98*, revision A.9; Gaussian, Inc.: Pittsburgh, PA, 1998.

(28) Becke, A. D. *J. Chem. Phys.* **1993**, *98*, 5648−5652.

(29) Lee, C.; Yang, W.; Parr, R. G. *Phys. Rev. B* **1988**, *37*, 785−789.

(30) Bianchi, R.; Casalone, G.; Simonetta, M. *Acta Crystallogr. B* **1975**, *31*, 1207−1209.

(31) Belci, M. Ph.D. Dissertation, Universität zu Köln, Köln, Germany, 1976.

(32) Nendel, M.; Houk, K. N.; Tolbert, L. M.; Vogel, E.; Jiao, H.; v. R. Schleyer, P. *J. Phys. Chem. A* **1998**, *102*, 7191−7198.

(33) Ketkar, S. N.; Kelley, M.; Fink, M.; Ivey, R. C. *J. Mol. Struct.* **1981**, *77*, 127−138.

(34) Nendel, M.; Houk, K. N.; Tolbert, L. M.; Vogel, E.; Jiao, H.; v. R. Schleyer, P. *Angew. Chem., Int. Ed. Engl.* **1997**, *36*, 748−750.

(35) Julg, A.; Francois, P. *Theor. Chim. Acta* **1967**, *8*, 249−259.

(36) Schrader, B. *Raman/Infrared Atlas of Organic Compounds*; VCH: Weinheim, Germany, 1989.